

Evaluation of performances of indexes used for validation of simulation models based on real cases

Jacopo Bongiorno and Andrea Mariscotti

Abstract—When simulation models are validated against experimental data, model adequacy and accuracy are evaluated using performance indexes that quantify distances between simulated and measured data vectors: amplitude, derivatives, slopes, peaks and valleys, etc. are all possible curve features. Performance indexes have appeared in the literature from different fields of science and are tested for suitability to problems involving electric networks. Indexes are evaluated for sensitivity to typical signal characteristics and the capability of detecting usual differences; tests are performed on synthetic and real cases.

Keywords—Electric networks, Modeling, Performance Index, Simulation, Validation

I. INTRODUCTION

NUMERIC models are being used more and more often for the assessment of system performance, reliability, safety in normal and exceptional conditions and configurations for a wide range of systems. Correspondingly, any simulation model needs a verification and validation process, that establishes its performance for the field of application [1]. Even limiting our scope to engineering and to electrical networks [2], control, operation, functionality, sizing, stability and distortion may all be analyzed in steady and transient conditions [3][4]. The first step is always to define the intended use and the required level of detail for the models and simulator building blocks, depending on the required task and objectives. Focusing on a specific type of electric networks, i.e. electric transportation systems, and on the phenomena usually evaluated for electrical interoperability, performance and electrical safety assessment, the required behavior is presented in the working documents of the CENELEC committee C20 [5]. The scope of this committee and its activities is the definition of a validation framework for railway simulators, recognizing different model categories, including mechanical and electrical infrastructure elements, a train electromechanical model, traffic information and the possibility of static and dynamic simulations. All these characteristics are subdivided between optional and required ones for different model categories, from category 1 to

category 4, the most complete. The use of numerical models is also suggested by the EU Directives on interoperability [6] and related standards for the evaluation of electrical interoperability [7].

For railway systems (and by extension any other electric transportation system) the relationship between safety and electromagnetic interference brings to very complex, expensive and time consuming assessment procedures. The latter benefit from, or are even unpractical without, adequate models of the system. This is readily explained if the possibility is considered of analyzing extreme system configurations and parameter values, and evaluating the statistical distributions of network response.

The verification of a model is the evaluation of the correspondence to the requirements, even for single modules during their development. The validation of a simulation model aims at verifying that it meets its intended use, in terms of overall requirements and user's expectations. The verification phase reviews intermediate elements, by means of static analysis techniques (inspections and reviews) and possibly dynamic techniques (execution of test runs of the simulator modules, maybe assisted by synthetic data). The whole validation process begins with the determination of the model type, its basic attributes and the relations with the system to be modeled. Then, when the model is being formulated and implemented, the model is validated by itself considering the expected model behavior. But the most relevant part of the validation process is represented by the characterization of the model accuracy with respect to the reference data. The validation of a simulator using dynamic techniques is performed by executing test runs on reference cases.

When using experimental data as reference, we must first consider that the data themselves are affected by measurement errors and are thus characterized by uncertainty. The term "error" is to be intended with a broad meaning, including internal and external noise, offsets and fluctuations, etc. that may affect the data and cause various types of aberrations and outliers.

The second relevant aspect is the completeness of the description of the physical system in terms of the selected

J. Bongiorno is with the University of Genova, 16145, Italy (e-mail: jacopo.bongiorno@edu.unige.it).

A. Mariscotti is with the University of Genova, 16145, Italy (phone: +390103532169; fax: +39010 3532700; e-mail: andrea.mariscotti@unige.it).

data. This is related to the accessibility of system variables (that at a different level of abstraction corresponds to system observability) and to the identification of the relevant ones.

Third, it is worth noting that additional sets of variables and parameters may be included in the validation, because of their “added value”, related to a more accurate and extended coverage of system dynamics, therefore increasing the detail of the system representation and of the validation outcome.

The data and simulator outputs mentioned so far are the electrical quantities of the system (namely voltage, current, impedance), taking the shape of time- or frequency-domain curves [8]. Curves in both domain have some distinct features, such as peaks and valleys, so positive and negative slopes, may be strictly positive (e.g. amplitude spectra) or crossing the zero axis (e.g. periodic time-domain signals), and might have a zero mean value. Time-domain signals are in general real valued, while spectra in frequency domain may be characterized in terms of amplitude and phase response.

When comparing simulated and experimental data of this kind several features normally capture the observer’s eye and may be used to quantify the degree of similarity. This work is focused on the suitability of known indexes of performance derived from other field of science. These indexes are applied to the simulation output comparing it to reference experimental results, that for our purpose are assumed accurate and characterized by a negligible uncertainty. The indexes that are considered and evaluated here were described in [9]; the objective is to evaluate the agreement or discrepancies between different indexes and methods, their applicability to the typical “signals” (indicating with this term both time-domain signals and frequency-domain spectra), the sensitivity to various types of errors between simulated and experimental results as differences in amplitude and displacement factor, for time domain models, and differences in amplitude, peaks position, peaks number, slope in frequency domain models.

To this aim errors and differences are artificially injected into synthetic signals, varying dc value, scale, phase differences, curve discontinuities, number of points.

II. PROBLEM FORMULATION

This work focuses on the indexes used to evaluate model adequacy and the degree of similarity between simulation and experimental data, where “similarity” indicates a quantitative evaluation of the distance between the two vectors o (simulation output) and m (measured data). Different distance metrics may be selected and applied as they appear in the indexes considered in the following: absolute deviation, maximum absolute deviation, root mean square, amplitude and slope difference, etc. Such metrics may be applied to the curves (point values) or to the first-order derivatives (slopes) or even to higher-order derivatives. The concepts of distance and correlation may be used to establish similarity between vectors. However, from a general viewpoint, when evaluating the correctness and adequacy of a simulation model, the

judgment is based on the visualization of many output results. Inspecting visually the results and basing the judgment upon this has its strong and weak sides:

- the eye concentrates on peak positions and ignores both the effective correlation of intensities and intervals with lower values;
- yet, visual evaluation selects the most relevant behavior and trend (such as slopes, peaks, curvature and convexity), rejecting many details with adverse influence (noise terms of different nature);
- an objective comparison between different groups of experts proved to be difficult, so that potentially the method is not 100% reliable;
- the amount and organization of data may be too large and complex to be compared visually with ease and in this case selection and feature extraction shall be implemented.

The five performance indexes, selected in [10] for the validation of the simulation model of 25 kV ac railway traction systems, are considered. They are tested, first, against synthetic signals with injected artificial errors and differences and, then, in sec. 4, they are evaluated with real case studies. The aim is to establish quantitatively the range of variation for the indexes, how to set their constants, which signal features are detected and evaluated best and worst by each index, and if the indexes have some weakness or inaccuracy with respect to some signal feature or class of signals.

A. Theil inconsistency coefficient [11]

The Theil inconsistency coefficient U is expressed in the following form:

$$U = \sqrt{\sum_{j=0}^{N-1} (o_j - m_j)^2} / \left[\sqrt{\sum_{j=0}^{N-1} o_j^2} + \sqrt{\sum_{j=0}^{N-1} m_j^2} \right] \quad (1)$$

U is limited between 0 and 1: the lower its value, the more consistent the two data vectors.

It is a classical root mean square error, normalized by the rms values of the o and m data vectors. It is very similar to the concept of normalized covariance of two distributions.

The Theil index is an amplitude-only index: by inspection of (1) it may be said that it has no singular points and that dc value and scale are not affecting its operation.

B. Zanazzi & Jona correlation factor [12]

Zanazzi and Jona correlation factor has been used in X-ray diffraction and surface crystallography and was designed to accentuate the slopes rather than the amplitudes, by comparing the first and second derivatives.

$$C = \sum_{i=0}^{N-1} m_i / \sum_{i=0}^{N-1} o_i \quad (2)$$

$$F_i = |C o_i' - m_i'| \quad (3)$$

$$W_i = \frac{|C o_i'' - m_i''|}{|m_i'| + |\max(m_i'')|} \quad (4)$$

$$R_{ZJ} = \sum_{i=0}^{N-1} W_i F_i / \sum_{i=0}^{N-1} m_i \quad (5)$$

where C is the ratio of averages to adjust the scale and R_{ZJ} is normalized to 1 for uncorrelated o and m vectors.

As it will be pointed out later on, the C coefficient is the weak point of the formulation, being exposed to zero mean data vectors (the mean value of o is at the denominator); in (5) also the mean value of m is at the denominator. So both equations are not definite for zero mean vectors.

Further susceptibility is of course related to the calculation of the first and second derivatives and to noise and discontinuities. No singular points of the denominator of (4) exist, because the $\max()$ term ensures that there is always a strictly positive value.

C. Pendry correlation factor [13]

The Pendry correlation factor is used instead when the two sequences have many variations (i.e. "peak and valleys"). The objective in [13] was to locate small peaks around large peaks, where the former could be masked by background noise; when transferred to electric networks this situation occurs when estimating highly damped non-dominant poles in the presence of strong resonances, or when identifying small narrowband components in the presence of a large fundamental or its main harmonics. By taking the fractional (or normalized) first derivative $L = x'/x$ of either the model output o or the experimental data m , the expression Y is built around it

$$Y = \frac{L^{-1}}{(L^{-2} + K^2)} \quad (6)$$

where K is a constant derived from the physical nature of the phenomenon and in general might be adjusted to trim the range of variation of L . The Pendry reliability index is thus defined in our case by distinguishing the Y calculated with model output Y_o and the one calculated with experimental results Y_m :

$$R_P = \sum_{i=0}^{N-1} (Y_o - Y_m)^2 / \sum_{i=0}^{N-1} (Y_o^2 + Y_m^2) \quad (7)$$

where the denominator normalizes the index again equal to 1 for uncorrelated o and m vectors.

Unlike R_{ZJ} , the R_P factor only requires the first derivative, making it less susceptible to small or rapid changes; this feature is useful for analyzing noisy sequences.

D. Modified Pendry correlation factor [14]

The use of the Pendry reliability factor R_P is strictly connected to the choice of the value to assign to the K constant (see (6)) furthermore, this index has no evident upper bound that establishes a range of values and a truly quantitative indexing of the goodness of fit for a certain class of problems.

To solve such problems a linear expression of the Pendry correlation factor, R_{PL} is proposed that limits the maximum variation of the index to 1, assuming a K constant equal to 0

$$R_{PL} = \sum_{i=0}^{N-1} |L_o - L_m| / \left(\sum_{i=0}^{N-1} |L_o| + |L_m| \right) \quad (8)$$

E. Van Hove correlation factor [15]

The Van Hove correlation factor is probably the most popular, with five different indexes to evaluate the position and width of the sequence peaks, the shape of the peaks and the valleys, their number and their amplitude.

$$R_{V1} = \sum_{i=0}^{N-1} |m_i - Co_i| / \sum_{i=0}^{N-1} |m_i| \quad (9)$$

$$R_{V2} = \sum_{i=0}^{N-1} (m_i - Co_i)^2 / \sum_{i=0}^{N-1} m_i^2 \quad (10)$$

$$R_{V3} = \frac{\#slopes^+(o)}{\#slopes^-(o)} - \frac{\#slopes^+(m)}{\#slopes^-(m)} \quad (11)$$

$$R_{V4} = \sum_{i=0}^{N-1} |m'_i - Co'_i| / \sum_{i=0}^{N-1} |m'_i| \quad (12)$$

$$R_{V5} = \sum_{i=0}^{N-1} (m'_i - Co'_i)^2 / \sum_{i=0}^{N-1} (m'_i)^2 \quad (13)$$

The five indices are synthesized in an overall indicator that takes the root square of the sum of the squares, without using any specific weighting of the single index:

$$R_V = \sqrt{R_{V1}^2 + R_{V2}^2 + R_{V3}^2 + R_{V4}^2 + R_{V5}^2} \quad (14)$$

This index suffers the same weakness related to the C coefficient commented in sec. II.B for the Zanazzi and Jona index. The other terms at denominator are all safe from a null value, because of the absolute values or square operators. It will be pointed out how the calculation of the number of slopes may lead to some discrepancy, being quite susceptible to approximations and round-offs at the extreme of the domain interval, when the number of peaks is small (and thus the number of positive and negative slopes). Furthermore, the algorithm needs a robust method to count the number of slopes, that at the moment is implemented using the `findpeaks()` function in Matlab.

F. IELF (integrated log-frequency) [16]

Going to problems of electromagnetic simulation, much closer to our topic, the Integrated against Error Log Frequency (IELF) index computes the difference between two traces in logarithmic horizontal scale and it is mostly suitable for frequency domain data. Its modified version is normally used, that takes the reference points halfway of each frequency bin and improves the approximation.

$$IELF = \frac{\sum_{i=0}^{N-1} |o_i - m_i| \left[\ln \frac{f_{i+1} + f_i}{2} - \ln \frac{f_{i-1} + f_i}{2} \right]}{\ln f_N - \ln f_0} \quad (15)$$

This index is extremely simple and thus quite reliable and stable. It has no numerical criticality.

III. TEST OF PERFORMANCE INDEXES

Quantitative tests have been made using a set of synthetic signals that possess the following characteristics: variable average value, constant and variable first derivative and discontinuities of the first derivative. The signals are all without added noise because it is commonly accepted and understood that the calculation of the first and higher order derivatives cannot be implemented satisfactorily if additive noise is present and curve smoothing is usually applied to prevent this.

The first test set is made of periodic signals that may be interpreted as signals in time domain: a sinusoid (case S) and a triangular (case T) signal of unitary amplitude, sampled at 200 kS/s, are used; the data vector are made of 10000 points. The differences between the reference vector m and the evaluated vector o are artificially obtained by shifting the two signals ("injected phase difference", IPD); being periodic, a shift of half period creates two signals with opposite amplitude values and slopes that represent the most different vectors. Phase is changed progressively from 45° , 90° to 180° .

Also the effect of an amplitude shift is considered and it was obtained by adding an offset ("injected offset", IOF). In this case an offset of 1 is added to bring the curve in the positive quadrant. This was done for two reasons: to test the effect of offsets, that do not change the scale but increase the maximum value, and to remove the problem of the zero mean on the coefficient C, that is common to the Zanazzi-Jona and Van Hove indexes; also for the Pendry index an offset is necessary because a zero mean brings the L coefficient to infinite.

When testing the frequency response of synthetic dynamic systems (that represent a large class of simulated systems), the changes applied to the pole values are of the parametric type, affecting the curve shape in its entirety and not only locally.

To this aim the frequency domain response of a dynamic system (case D) with two complex conjugate poles with resonance frequency $f_n=7000$ Hz and damping factor $\xi=0.2$ was used. Then the dynamic system underwent a parametric change, moving the poles by given quantities obtained by adding or subtracting to the real and imaginary part a percentage of the absolute value (the undamped resonant frequency). This method is "dynamic system deterministic", or DD, and applies in the specific case a variation of the pole in six step, summing and subtracting, to the real and imaginary part of the pole, 1, 1/2, 1/4 of the 1 or 10% of his absolute value. Moreover, in order to verify the dependence of the indexes to the absolute value of the curves this was changed using a static gain of 2 and 4.)

A more complete evaluation is then performed with a statistical approach, or DS, applying a random change of the pole values by Monte Carlo analysis; the random pole movement was set to a Gaussian distribution with zero mean value and dispersion of 1 and 10% of the pole absolute value (again the resonant frequency f_n , or pulsation $2\pi f_n$). The results are displayed as histograms of the probability density

function (pdf), together with the estimation of the mean value μ and standard deviation σ of the sample.

The resulting performances are reported in the following subsections for each index.

A. Theil

As evidenced in Table 1 the value of the index is strongly influenced by the amplitude of the curves: the statement that the range of variation of the index is at most between 0 and 1 is true if the mean value of the curves to compare is zero, so that the dc component must be removed from the data vector before comparison. However, the index values are consistent with the injected difference, decreasing uniformly for decreasing phase difference.

Table 1. Theil index for the sinusoidal and triangular curves test

	ph.displ.= π		ph.displ.= $\pi/2$		ph.displ.= $\pi/4$	
	off=0	off=2	off=0	off=2	off=0	off=2
S	1.00	0.23	0.71	0.16	0.38	0.09
T	1.00	0.38	0.70	0.26	0.40	0.10

The Theil inconsistency index has no scale problems and is independent on the amplitude of the curves, as shown in Table 2.

Table 2. Theil index for the dynamic system deterministic test (DD)

pole step	1% ω_n		10% ω_n	
	$G_0=2$	$G_0=4$	$G_0=2$	$G_0=4$
+1	0.013	0.013	0.098	0.098
-1	0.014	0.014	0.191	0.191
+1/2	0.006	0.006	0.056	0.056
-1/2	0.007	0.007	0.078	0.078
+1/4	0.003	0.003	0.030	0.030
-1/4	0.003	0.003	0.036	0.036

The Theil index is linear, hence its distribution is the result of the quadrature composition of the two Gaussian distributions for the real and imaginary part of the poles: the resulting pdf is a Rayleigh as it appears from Fig. 1 and Fig. 2. The linearity is confirmed by the ten times larger mean and dispersion values when the 10% random variation is applied.

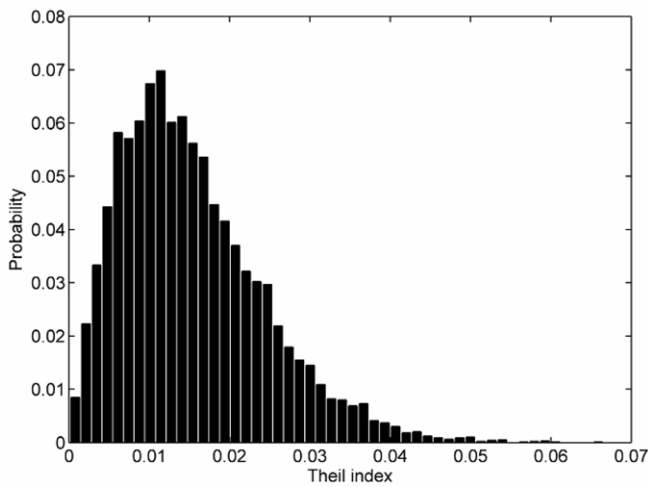


Fig. 1. Theil pdf for 1% DS ($\mu=0.0153, \sigma=0.0089$)

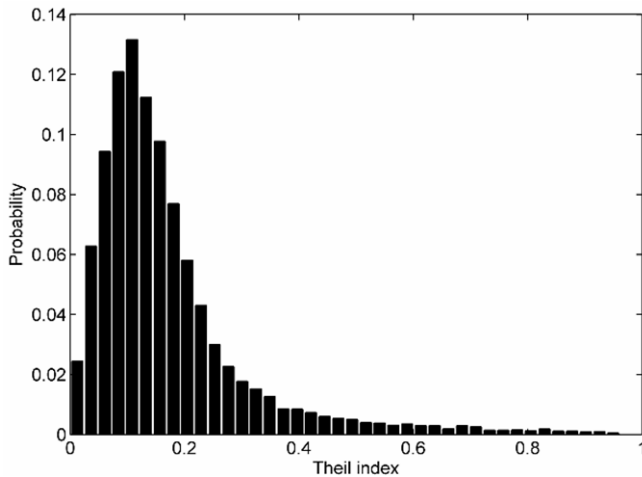


Fig. 2. Theil pdf for 10% DS ($\mu=0.171, \sigma=0.139$)

B. Zanazzi-Jona

This index needs a strong customization to the specific problem before being used satisfactorily. The original index is quite related to the class of problems for which it was conceived: the scaling factor C shown in (2) prohibits to evaluate curves with zero mean value, like most of periodic time domain signals and oppositely to the previous Theil index; the index is also unsuitable for curves with discontinuities in the first derivative or second derivative, as the triangular test signal. This problem may occur also in frequency domain data when a spectrum shows a resonance peak with quite a small damping. When the frequency resolution is constrained by practical issues, even moderate Q factors may cause numeric discontinuities for particularly unlucky distributions of the frequency axis points with respect to the original continuous frequency resonance.

Furthermore, this index has no evident upper bound that establishes a range of values and a truly quantitative indexing of the goodness of fit for a certain class of problems: it indicates simply how close or far are two data vectors and the

index can only be used to establish which data vector \mathbf{o} of a set is more similar to the reference data vector \mathbf{m} . To this aim the index may be scaled assigning 1 to the worst value obtained for the least fit vector of the set. Zanazzi & Jona propose to normalize the index with respect to the mean of N vectors, even obtained by random variations around an original vector, obtaining what he calls “Reduced Reliability Index” [12].

Table 3. Zanazzi-Jona index for the sinusoidal and triangular curves test

	ph.displ.= π		ph.displ.= $\pi/2$		ph.displ.= $\pi/4$	
	off=1	off=2	off=1	off=2	off=1	off=2
S	$8.34 \cdot 10^3$	$4.17 \cdot 10^3$	$4.42 \cdot 10^3$	$2.22 \cdot 10^3$	$1.18 \cdot 10^3$	$0.59 \cdot 10^3$
T	$2.53 \cdot 10^3$	$1.52 \cdot 10^3$	$1.33 \cdot 10^3$	$0.80 \cdot 10^3$	$1.33 \cdot 10^3$	$0.80 \cdot 10^3$

Also the Zanazzi-Jona reliability index R_{ZJ} is not scale sensitive, as shown in Table 4.

Table 4. Zanazzi-Jona index for the dynamic system deterministic test (DD)

pole step	1% ω_n		10% ω_n	
	$G_0=2$	$G_0=4$	$G_0=2$	$G_0=4$
+1	$8.41 \cdot 10^{-6}$	$8.41 \cdot 10^{-6}$	$5.09 \cdot 10^{-4}$	$5.09 \cdot 10^{-4}$
-1	$9.27 \cdot 10^{-6}$	$9.27 \cdot 10^{-6}$	$13.7 \cdot 10^{-4}$	$13.7 \cdot 10^{-4}$
+1/2	$2.15 \cdot 10^{-6}$	$2.15 \cdot 10^{-6}$	$1.69 \cdot 10^{-4}$	$1.69 \cdot 10^{-4}$
-1/2	$2.26 \cdot 10^{-6}$	$2.26 \cdot 10^{-6}$	$2.76 \cdot 10^{-4}$	$2.76 \cdot 10^{-4}$
+1/4	$0.55 \cdot 10^{-6}$	$0.55 \cdot 10^{-6}$	$0.49 \cdot 10^{-4}$	$0.49 \cdot 10^{-4}$
-1/4	$0.56 \cdot 10^{-6}$	$0.56 \cdot 10^{-6}$	$0.62 \cdot 10^{-4}$	$0.62 \cdot 10^{-4}$

The Zanazzi-Jona index applied to the synthetic curves is insensible to the static gain variation of them. The index however recognize the curves closer to the reference one even if, as said above, the absence of a sure interval of variation of the index make it useful only for relative, and not absolute, assessment.

The Monte Carlo analysis is repeated also for the Zanazzi-Jona index, that is known to be non-linear. The output passing from the 1% to the 10% applied perturbation spread dramatically and for the largest perturbation the pdf is displayed on a log distributed abscissa.

The statistical analysis shows the non linearity of the Zanazzi-Jona index and the unsuitability to distinguish curves with large differences between them. The spread of index values for just a 10% standard deviation of the Gaussian random variable is amazing, yet with misleading limited values of the mean and dispersion of the index.

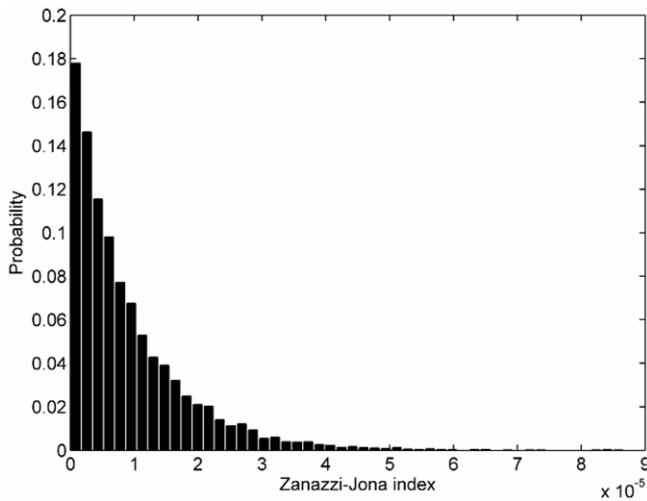


Fig. 3. Zanazzi-Jona pdf for 1% DS ($\mu=9.12 \cdot 10^{-6}$, $\sigma=9.22 \cdot 10^{-6}$)

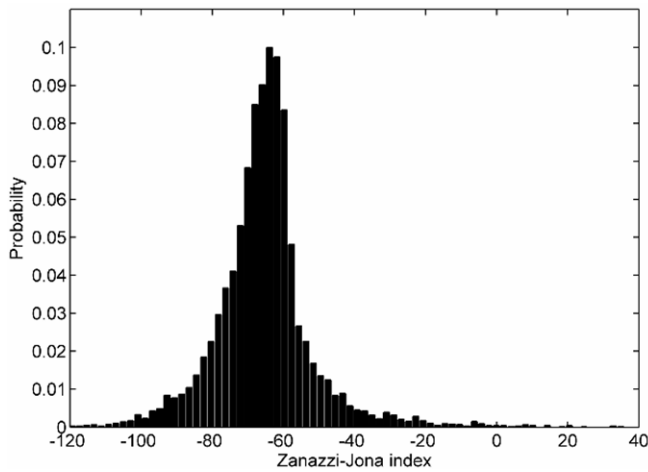


Fig. 4. Zanazzi-Jona pdf for 10% DS ($\mu=0.051$, $\sigma=1.87$)

C. Pendry

The use of the Pendry reliability factor R_P is strictly connected to the choice of the value to assign to the K constant (see (6)). The index is undefined for curves with zero data samples; this does not occur for the curves for which it was originally conceived and may thus be applied to the vast class of frequency domain spectra, provided that only the amplitude, and not the phase, is evaluated.

The application of this index for the validation of electromagnetic models was investigated in [17], where the K factor was omitted, simplifying a lot (6); eq. (7) thus becomes

$$R_P = \frac{\sum_{i=0}^{N-1} (L_o - L_m)^2}{\sum_{i=0}^{N-1} (L_o^2 + L_m^2)} \quad (16)$$

The authors in [17] indicate a range of variation between 0 and 1, but as shown in Table 5 the index assumes in reality also values larger than one!

Removing the factor K , however, has the drawback that the index now depends strongly on the data vector amplitude.

Furthermore, it also does not allow the comparison of curves for which the first derivative is zero, even for a fraction of their domain.

Using R_{PL} (8) saturation to unity for extremely different curves is assured, as shown in Table 5.

Table 5. Pendry and modified Pendry indexes for the sinusoidal and triangular curves test

		ph.displ.= π		ph.displ.= $\pi/2$		ph.displ.= $\pi/4$	
		off=0	off=2	off=0	off=2	off=0	off=2
S	R_P	1.84	1.94	1.07	1.03	0.35	0.31
	R_{PL}	1.00	1.00	0.72	0.71	0.40	0.39
T	R_P	1.92	1.97	1.02	1.01	0.55	0.51
	R_{PL}	1.00	0.38	0.59	0.55	0.32	0.29

The modified Pendry index R_{PL} works fine with a smoother and more proportional change depending on the injected phase difference; the maximum is 1 whatever the amplitude of the curves, increasing its reliability and the applicability.

Table 6. Pendry and modified Pendry indexes for the dynamic system test (DD)

		1% ω_n		10% ω_n	
pole step		$G_0=2$	$G_0=4$	$G_0=2$	$G_0=4$
R_P	+1	$5.16 \cdot 10^{-6}$	$2.05 \cdot 10^{-4}$	$2.84 \cdot 10^{-4}$	$1.11 \cdot 10^{-3}$
	-1	$5.99 \cdot 10^{-6}$	$2.38 \cdot 10^{-5}$	$13 \cdot 10^{-4}$	$5.33 \cdot 10^{-3}$
	+1/2	$1.34 \cdot 10^{-6}$	$5.31 \cdot 10^{-5}$	$0.97 \cdot 10^{-4}$	$0.39 \cdot 10^{-3}$
	-1/2	$1.44 \cdot 10^{-6}$	$5.73 \cdot 10^{-5}$	$2.07 \cdot 10^{-4}$	$0.82 \cdot 10^{-3}$
	+1/4	$0.34 \cdot 10^{-6}$	$0.13 \cdot 10^{-5}$	$2.89 \cdot 10^{-4}$	$0.12 \cdot 10^{-3}$
	-1/4	$0.35 \cdot 10^{-6}$	$0.14 \cdot 10^{-5}$	$4.22 \cdot 10^{-4}$	$0.17 \cdot 10^{-3}$
R_{PL}	+1	0.0223	0.0248	0.2057	0.2328
	-1	0.0227	0.0251	0.2489	0.2695
	+1/2	0.0112	0.0124	0.1079	0.1209
	-1/2	0.0113	0.0125	0.176	0.1289
	+1/4	0.0056	0.0062	0.0551	0.0615
	-1/4	0.0056	0.0063	0.0575	0.0634

Observing the Pendry index values calculated for the synthetic curves and reported in Table 6, it is evident the dependency of the index on the overall amplitude of the curves (static gain): the larger the gain the larger the index, yet with a moderate sensitivity.

The modified Pendry index has quite a consistent behavior by indicating similar values for changes in poles of opposite sign but equal amplitude. It is moreover proportional to the amplitude of the step change, doubling while passing from 1/4 to 1/2 and then 1. Analogously when the fractional change passes from 1% to 10% we observe an increase of an order of magnitude in the R_{PL} index. The original Pendry index has much larger variations and is quite susceptible to scale changes, while the modified version shows a modest variation of less than 10% when the static gain doubles.

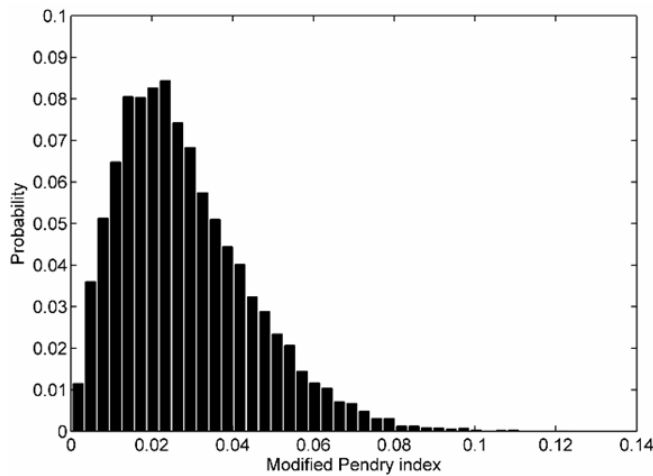


Fig. 5. Modified Pendry R_{PL} pdf for 1% DS ($\mu=0.0283$, $\sigma=0.0165$)

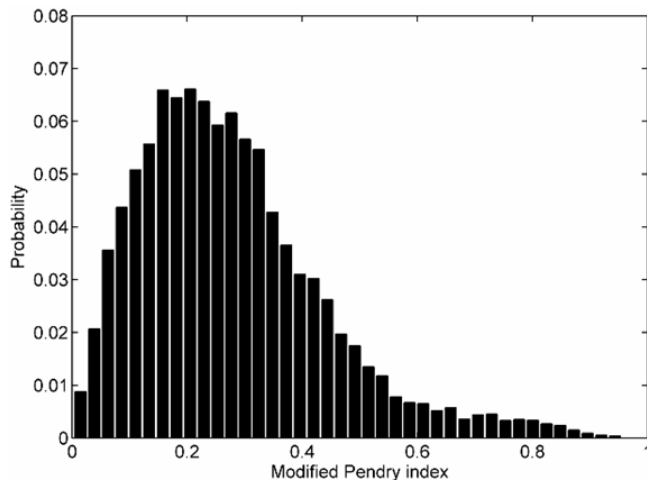


Fig. 6. Modified Pendry R_{PL} pdf for 10% DS ($\mu=0.277$, $\sigma=0.162$)

The modified Pendry index is linear and, as for Theil index the resultant distribution is similar to a Rayleigh distribution. The linearity is confirmed by the exact ten times larger mean and dispersion. The shape of the pdf is however deviates slightly from the expected Rayleigh for the largest perturbation: the reason might be related to the statistical significance of the 10000 samples for the Monte Carlo analysis or to second order effect of the proposed R_{PL} index. This aspect is still under investigation.

D. Van Hove index

Van Hove separates the evaluation of various features of the curves by assigning a different index of a set of five: absolute deviation of amplitude, mean square error of amplitude, slope change, absolute deviation of the first derivative and mean square error of the first derivative. In this way the differences between the input data vectors are better evaluated. The overall index R_V is built around the square root of the sum of the squares of the five indexes. The author does not propose any weighting of an index with respect to another,

keeping them all with a unity multiplying coefficient.

Much similar curves in slope and amplitude may differ for local artifacts of the first derivative, resulting in this way quite different if the overall index alone is taken. This is shown better looking at R_{V4} and R_{V5} indexes in Table 7; hence if just only one of the sub-indexes assumes wrong or weird values, the overall index give a unreliable indication of large difference of the compared curves.

In order to widen the applicability of the Van Hove index, in particular when periodic/oscillatory signals are evaluated, it is proposed to calculate the R_{V1} and R_{V2} sub-indexes removing any signal offset, limiting the value of the sub-indexes to unity; the other sub-indexes may still be calculated on the original signals.

When there is only one peak in the curves, the R_{V3} index cannot be calculated; in general, with a reduced number of peaks, missing one peak at the extreme of the frequency interval, strongly influence the result. The R_{V3} index has turned out to be quite unreliable and was for this reason omitted from the calculation of the overall index, that is thus made only of R_{V1} , R_{V2} , R_{V4} and R_{V5} .

Table 7. Van Hove index for the sinusoidal and triangular curves test

		ph.displ.= π		ph.displ.= $\pi/2$		ph.displ.= $\pi/4$	
		off=1	off=2	off=1	off=2	off=1	off=2
S	R_V	4.84	4.50	2.70	2.48	1.10	0.98
	R_{V1}	1.27	0.42	0.90	0.30	0.49	0.16
	R_{V2}	1.33	0.21	0.67	0.11	0.20	0.03
	R_{V3}	0	0	0.20	0.20	0	0
	R_{V4}	2.00	2.00	1.41	1.41	0.77	0.77
	R_{V5}	4.00	4.00	2.00	2.00	0.59	0.59
T	R_V	4.71	4.50	2.42	2.25	1.24	1.15
	R_{V1}	1.00	0.14	0.75	0.11	0.44	0.06
	R_{V2}	1.00	0.03	0.50	0.01	0.16	0.00
	R_{V3}	0.45	0.45	0.25	0.25	0.25	0.25
	R_{V4}	2.00	2.00	1.00	1.00	0.50	0.50
	R_{V5}	4.00	4.00	2.00	2.00	1.00	1.00

Regarding the linearity and the sensitivity to the curve scale, for the Van Hove index we may say that: as for the Zanazzi-Jona index the amplitude of the synthetic curves does not influence the index value; the index is non-linear with respect to the applied changes, but its behavior is consistent, making correspond increase with increase in a moderately proportional way.

In Table 8 the results for the tests performed with the simulated dynamic system are shown; as anticipated the overall index R_V is calculated excluding R_{V3} . As for the modified Pendry index there is consistent behavior with equal or much similar values for changes in poles of opposite sign but equal amplitude. Also it is proportional to the amplitude of the step change, doubling while passing from 1/4 to 1/2 and then 1. When the fractional change passes from 1% to 10% there is an increase of the index value of about 12 rather than the expected 10. Finally, the index is not sensitive to the curve

scale, as it is demonstrated doubling the static gain.

Table 8. Van Hove index for the dynamic system deterministic test (DD)

		1% ω_n		10% ω_n	
pole step		$G_0=2$	$G_0=4$	$G_0=2$	$G_0=4$
R_V	+1	0.0739	0.0739	1.2334	1.2334
	-1	0.0731	0.0731	0.9544	0.9544
	+1/2	0.0367	0.0367	0.4386	0.4386
	-1/2	0.0365	0.0365	0.4089	0.4089
	+1/4	0.0183	0.0183	0.1931	0.1931
	-1/4	0.0182	0.0182	0.1879	0.1879
R_{V1}	+1	0.0170	0.0170	0.1291	0.1291
	-1	0.0182	0.0182	0.2506	0.2506
	+1/2	0.0087	0.0087	0.0751	0.0751
	-1/2	0.0090	0.0090	0.1042	0.1042
	+1/4	0.0044	0.0044	0.0406	0.0406
	-1/4	0.0044	0.0044	0.0478	0.0478
R_{V2}	+1	0.0004	0.0004	0.0256	0.0256
	-1	0.0005	0.0005	0.0887	0.0887
	+1/2	0.0001	0.0001	0.0086	0.0086
	-1/2	0.0001	0.0001	0.0160	0.0160
	+1/4	0.0000	0.0000	0.0025	0.0025
	-1/4	0.0000	0.0000	0.0034	0.0034
R_{V4}	+1	0.0714	0.0714	0.7819	0.7819
	-1	0.0703	0.0703	0.6491	0.6491
	+1/2	0.0356	0.0356	0.3692	0.3692
	-1/2	0.0353	0.0353	0.3414	0.3414
	+1/4	0.0177	0.0177	0.1806	0.1806
	-1/4	0.0177	0.0177	0.1739	0.1739
R_{V5}	+1	0.0087	0.0087	0.9448	0.9448
	-1	0.0085	0.0085	0.6472	0.6472
	+1/2	0.0022	0.0022	0.2244	0.2244
	-1/2	0.0021	0.0021	0.1989	0.1989
	+1/4	0.0005	0.0005	0.0551	0.0551
	-1/4	0.0005	0.0005	0.0523	0.0523

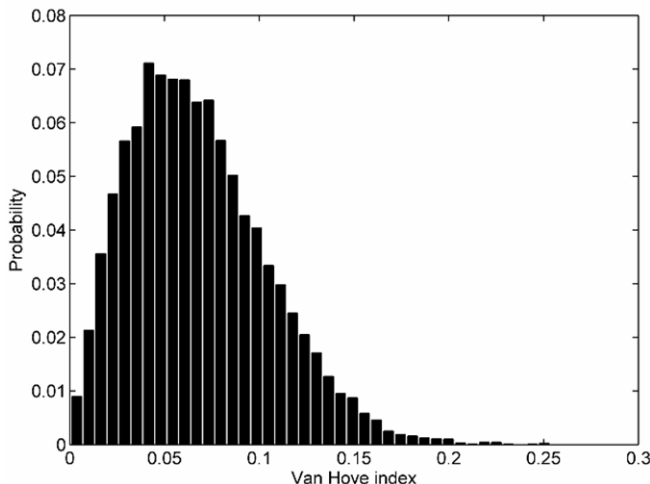


Fig. 7. Van Hove R_V pdf for 1% DS ($\mu=0.0681$, $\sigma=0.0365$)

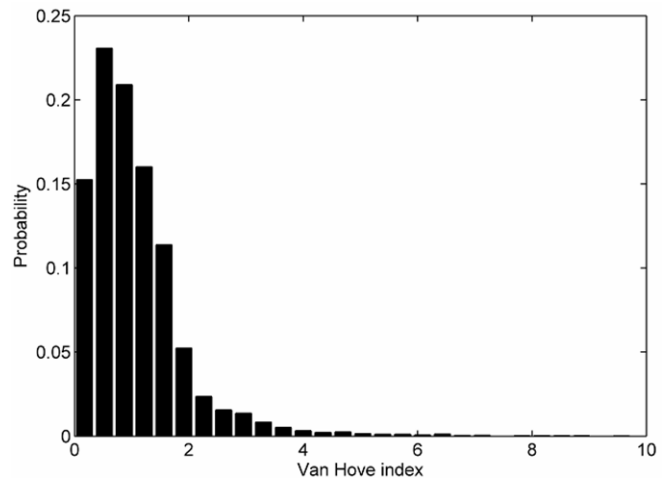


Fig. 8. Van Hove R_V pdf for 10% DS ($\mu=1.066$, $\sigma=0.873$)

Observing the histogram of the Van Hove overall index R_V , it can be noticed a slight non-linearity, getting worse with the increase of the applied perturbation.

E. IELF

The analysis of IELF index for periodic signals shows its insensibility to the amplitude of the curves. When tracked with respect to the injected difference, whilst for the triangular signal the behavior is monotonic, for the sinusoidal curve the largest difference is detected when the phase difference is $\pi/2$. Inspecting the IELF formulation given in (14) does not show any clue. A mutual effect between the phase reversal of the difference and the logarithmic distribution of points around singularities may be identified as a possible cause; nothing relevant, however, was resulting from the first tests.

Table 9. IELF index for the sinusoidal and triangular curves test

	ph.displ.= π		ph.displ.= $\pi/2$		ph.displ.= $\pi/4$	
	off=0	off=2	off=0	off=2	off=0	off=2
S	0.722	0.722	0.921	0.921	0.617	0.617
T	0.800	0.800	0.427	0.427	0.221	0.221

Table 10. IELF index for the dynamic system deterministic test (DD)

		1% ω_n		10% ω_n	
pole step		$G_0=2$	$G_0=4$	$G_0=2$	$G_0=4$
+1		0.0105	0.0209	0.0785	0.1571
-1		0.0113	0.0225	0.1649	0.3298
+1/2		0.0053	0.0107	0.0458	0.0916
-1/2		0.0055	0.0110	0.0657	0.1314
+1/4		0.0027	0.0054	0.0249	0.0497
-1/4		0.0027	0.0055	0.0298	0.0595

As for the modified Pendry index, there is a consistent behavior with equal or much similar values for changes in poles of opposite sign but equal amplitude. Also the IELF

index is proportional to the amplitude of the step change, doubling while passing from 1/4 to 1/2 and then 1. When the fractional change passes from 1% to 10% there is an increase of the index value of about 7 rather than the expected 10 (it is thus slightly non-linear as the Van Hove index). Here, doubling the static gain doubles the index value, so indicating sensitivity to the curve scale.

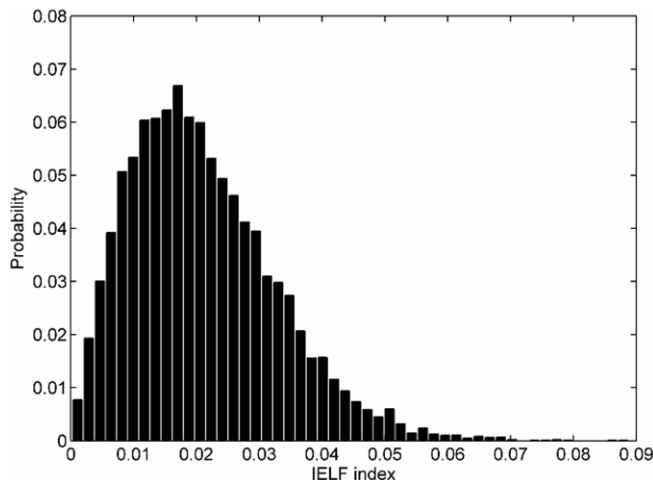


Fig. 9. IELF pdf for 1% DS ($\mu=0.021$, $\sigma=0.0116$)

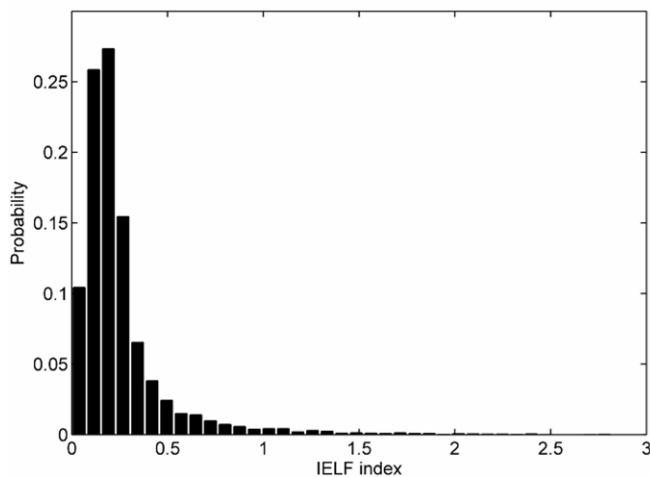


Fig. 10. IELF pdf for 10% DS ($\mu=0.254$, $\sigma=0.256$)

As for Van Hove overall index R_V , also the IELF index has a slight increase “larger than expected” of the dispersion, that however keeps under control.

IV. APPLICATION TO REAL CASE STUDIES

As already pointed out in the Introduction, noise always affects measurement results, causing random fluctuations, outliers, local waveshape aberrations: several forms of filtering and smoothing are necessary, provided that they do not cause information loss or uncertainty increase. When using indexes based on the estimation of the first or second derivative, noise removal is particularly important and compulsory.

Moreover, measured and simulated data shall be made homogeneous for representation, number of samples, sample rate and so on, to allow a direct comparison.

Two railway lines are considered as an example: the first one is a test ring in Czech Republic used for rolling stock homologation in Europe and was studied extensively for some days leading to quite an accurate model; the second one is part of the Italian high-speed network and the information is limited to design documents and general characteristics of devices and apparatus.

A. Velim test ring, Czech Republic

In this case it was possible to evaluate the influence on model accuracy of some second-order parameters. The study was performed within the European Project EUREMCO, undergoing two days of preliminary measurements of the electrical characteristics of the test ring, testing open and short circuit configurations.

The Velim test centre has two test rings: the smaller one has a length of 6 km and is surrounded by the bigger one that is about 13.2 km long. The inner ring is not included in the model because during the measurement it was sectioned, but it might influence the outer ring subject to measurements because of coupling through the return circuit. The big test ring is composed of six conductors along its length.

Rails are connected together (transversal bonding) every 300 m, except in the track circuit testing area between chainage 10.672 and 11.672; the two catenary (positive) feeders are connected with the contact line and messenger every 120 m

Low voltage measurements were performed to characterize the test ring, using two different configurations (open-circuit, OC, and short-circuit, SC) to fit the 1-day time slot available. In the ideal case of an ideal transmission line the responses for the two configurations may be calculated one from the other. A railway line has frequency-dependent losses and inductance of the return circuit, small non-linearities and its response is influenced by connected equipment (e.g. power transformers) and leakage to earth, including the coupling to other earthed installations (as it is the case for the small ring partially coupled to the big ring). Moreover, the substation and the feeding cable need their own modeling, as well as the circuit used during the test to feed the excitation signal. Last, inductive coupling by nearby overhead transmission lines worsens the measured signal quality at very low frequency, thus requiring to set the lowest frequency above the supply fundamental at 50 Hz.

The tested frequencies are between 100 Hz and 20 kHz, with a suitable frequency step; the excitation signal is swept over this frequency interval and the relevant quantities (voltages and currents) are acquired by means of data acquisition systems. The frequency analysis is done with a Fourier transform approach, using a Hann smoothing window to reduce the frequency leakage and a preliminary estimate of the exact applied frequency to allow for synchronous extraction of the time epoch T_w to transform. A first

instantaneous frequency estimate, made using an approximate T_w based on the nominal frequency value, allows the fine adjustment of T_w trimming the number of samples N , with a time resolution given by the inverse of the sampling frequency. Symmetric zero-padding is used to artificially improve the frequency resolution during the Fourier analysis.

The visual comparison is made first on the simulated values using standard values of network elements and parameters, such as rail impedance, losses and parasitics of the circuit setup, rail-to-earth conductance. Then the model is refined, including measured values for some parameters, and sensitivity analysis is performed when assigned parameter values are variable or uncertain. The identified parameters suitable for sensitivity analysis are: supply cable capacitance C_c and losses, identified with the transversal conductance G_c ; rail-to-earth conductance G_r ; rail longitudinal resistance R_r . The nominal values used as reference are derived from datasheets (e.g. normal values for cables of the same cross-section and same rated voltage) or by published measurements [18][19].

Besides a general check on the voltage and current levels to match simulated and measured values, the line input impedance is used for the validation, ruling out any amplitude error in the fine adjustment of the feeding voltage and resulting current (as already explained in [8][10]). The input impedance curves for the SC and OC configurations are shown in Fig. 11 and Fig. 12 for different parameter settings. The performance indexes for the same curves are evaluated and results reported in Table 11 and Table 12.

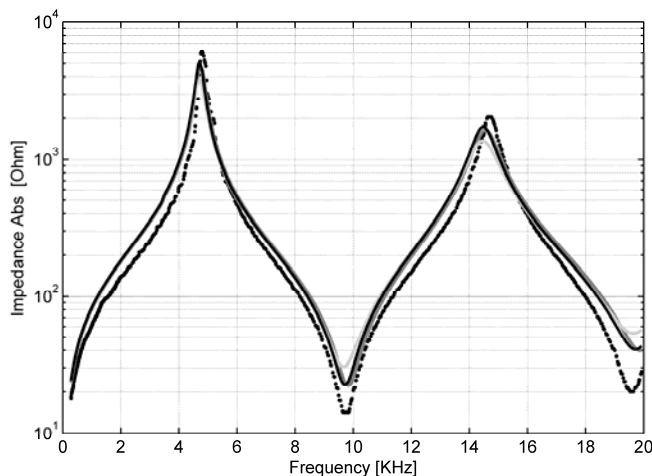


Fig. 11. SC configuration: (light gray) $G_r=50 \mu\text{S/m}$, $C_c=130 \text{ pF/m}$, (dark gray) $G_r=500 \mu\text{S/m}$, (black) $G_r=100 \mu\text{S/m}$, halved R_r , (black dots) measured values

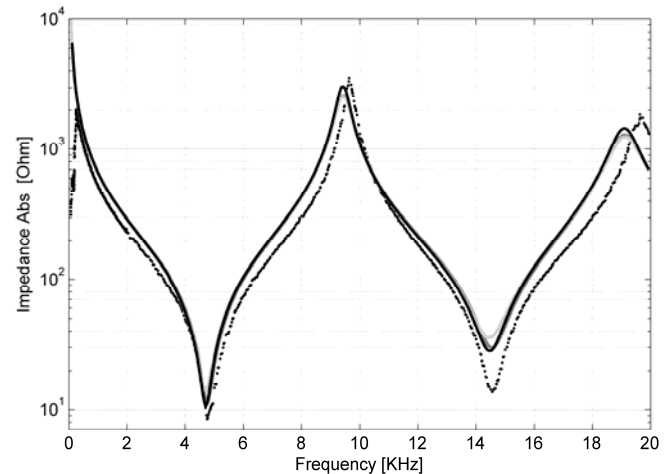


Fig. 12. OC configuration: (light gray) $G_r=50 \mu\text{S/m}$, $C_c=130 \text{ pF/m}$, (dark gray) $G_r=500 \mu\text{S/m}$, (black) $G_r=100 \mu\text{S/m}$, halved R_r , (black dots) measured values

In Fig. 11, the dark gray and black curves were obtained in an attempt to include the effect of the internal ring that couldn't be tested or measured. The return circuits are connected through the soil and the earthing system thus lowering the rail equivalent longitudinal resistance and increasing the rail-to-earth conductance.

Considering the anti-resonance of the SC impedance at 10 kHz, the larger simulated value indicates a larger longitudinal resistance, that is larger losses in the running rails model. It is however to be underlined that losses in the rails at such a large frequency are subject to huge variations in any case from sample to sample, because electric losses are not controlled as a qualifying parameter during the production of rails. There are only half a dozen works in one century on this topic, only three if audiofrequency is considered; in [19] the spread of measured values for a single rail sample is already in the order of 20%, but between different rails even of the same gauge and type it might be much larger.

The same considerations are true also for Fig. 12 where the results for the open circuit configuration are shown. It is underlined that at low frequency, below about 400 Hz, the input current is very small and the recorded signal is quite noisy, causing data corruption, seen as the extremely low impedance values at the beginning of the curve. For this reason the frequency interval up to 400 Hz is displayed but excluded from the comparison and calculation of indexes.

For both configurations a visual analysis concludes that the simulated curves including the effects of the internal ring in parallel are the closest to the measured results.

In Table 11 and Table 12 we report the performance indexes calculated for the different parameter combinations; the Pendry index R_p couldn't be calculated because of a null derivative in at least one point.

Table 11. Short Circuit configuration: index values for the three simulation cases of Fig. 11

		$G_r=50 \mu\text{S/m}$	$G_r=500 \mu\text{S/m}$	$G_r=50 \mu\text{S/m}$ $R_r=50\%$
Theil		0.2470	0.1592	0.1949
Pendry	R_P	-	-	-
	R_{PL}	0.6791	0.6856	0.6865
Van Hove	RV	1.3132	1.1817	1.2338
	RV_1	0.3278	0.2160	0.2521
	RV_2	0.1588	0.0869	0.1193
	RV_3	0	0	0
	RV_4	0.8550	0.7774	0.8187
	RV_5	0.9277	0.8590	0.8800
Z-J		18.096	19.211	18.835
IELF		115.23	94.3788	110.688

Table 12. Open Circuit configuration: index values for the three simulation cases of Fig. 12

		$G_r=50 \mu\text{S/m}$	$G_r=500 \mu\text{S/m}$	$G_r=50 \mu\text{S/m}$ $R_r=50\%$
Theil		0.1723	0.1719	0.1823
Pendry	R_P			
	R_{PL}	0.8479	0.8449	0.8571
Van Hove	RV	1.4231	1.4229	1.4204
	RV_1	0.1924	0.1883	0.1827
	RV_2	0.1120	0.1104	0.1050
	RV_3	0	0	0
	RV_4	0.9903	0.9910	0.9891
	RV_5	0.9975	0.9975	0.9974
Z-J		5.9e3	6.0e3	6.3e3
IELF		127.19	128.01	153.12

Observing the results listed in table the second impedance curve, with an increased conductance seems to be the best fit to the measurement, followed by the third curve.

Van hove indexes shown that the main differences between measurements and simulation are in first derivative terms, while a good agreement is reached for punctual values of the amplitude of the curves and a perfect match is obtained regarding the number of the peaks.

Zanazzi Jona index, that consider also second derivatives terms, give some discordant indication respect the other indexes because it indicate the closest curve as the first one both for open circuit and short circuit configurations. In case of short circuit configuration also the IELF index indicate the first curve as the best.

The two indexes that can be considered for absolute considerations, because they have a limit in value, are discordant: Theil index is very low, indicating that the curves

are close to the measurement one. Modified Pendry index however is over the 0.5 and this fact indicates that the curves are not so close. Considering Theil index for the best fit curve in both configurations it can be noticed that short circuit simulation fits measurement better than open circuit simulation. This behavior is confirmed observing Modified Pendry index for the same curves; however the difference of values of this index is higher than for Theil index and it indicate a major difference between derivative terms of open circuit simulation and measurement.

In Table 13 the maximum absolute error, the mean absolute error and the root mean square between measurement and simulated curves are presented.

Table 13. Classical errors for the Short Circuit and Open Circuit configurations: maximum absolute error (max), mean absolute error (mean) and root mean square error (rms)

		$G_r=50 \mu\text{S/m}$	$G_r=500 \mu\text{S/m}$	$G_r=50 \mu\text{S/m}$ $R_r=50\%$
short circuit	max	2840	1670	2040
	mean	113.3	91.3	106.3
	rms	325.3	211.0	265.2
open circuit	max	1500	1470	1420
	mean	144.1	144.4	159.4
	rms	236.0	236.6	268.7

B. Italian high-speed line (Turin-Milan)

A more complicate system response is considered as real study case. Test runs of a locomotive were made on the Italian 2x25 kV high-speed line to verify the line influence on the rolling stock conducted emissions. The study was performed within the European Project EUREMCO as a contribution to CENELEC activities of standardization of the testing and evaluation of rolling stock disturbance to signaling circuits.

Several sources are present in a real line, including substations besides rolling stock, all in different and varying operating conditions. Again the pantograph impedance (the ratio of the pantograph voltage and current [8]) is selected as the reference quantity for the validation. This is a real case with partial information and is used for the evaluation of the performance indexes and simulator performance.

Raw measured data were sampled at 50 kS/s and Fourier transformed over $T_w=100$ ms windows, again using a Hann window and 50% of overlap for a total of 9 windows over a time interval of 0.5 s, which is used for averaging, to reduce the measurement noise (uncorrelated noise). When calculating the pantograph impedance by rationing voltage and current spectra, only odd harmonics of the 50 Hz fundamental are used, that are known to be characteristic harmonics: among them, the low order ones are normally influenced by the supply, while above about 1 kHz rolling stock influence is much more relevant.

The model of the line was based on technical drawings and nominal values of devices and elements, without the

possibility of dedicated tests. It is thus expected that the fitting is worse, and this shows up as inaccuracy in peak location and – as before in the first case – inaccurate estimation of losses (see Fig. 13). The attention is focused as in a real situation on the most important elements that are approximately known (see the rail parameters discussed before); other infrastructure variations are more difficult to track, if they are not documented and inspected one by one. The considered parameters and their intervals of variation are the following:

- Length of feeding cables between substation and line; all substations are quite directly connected to the line, but differences of less than 50 m were found relevant; the cables are normally arranged as two in parallel; so 75, 150, 225 and 300 m of length with two cables in parallel are tested with rail-to-earth conductance of 500 $\mu\text{S/m}$ (cases L1, L2 and L3 in Table 14)
- Rail-to-earth conductance should be lower because the line is relatively new, but even the change of moisture between day and night might have a significant effect; the 500 $\mu\text{S/m}$ value assumed above is quite a large value, justified by some leakage through the sleepers typical of that part of the Italian network; however, lower values are more likely to occur, such as $G_1=5 \mu\text{S/m}$ and $G_2=50 \mu\text{S/m}$, fixing the length of the feeding cables to 150 m (see Table 15).

The indexes are thus calculated, taking as reference the measurement impedance curve.

Focusing on a visual analysis looking at Fig. 13 the difficulty is evident to choose the best simulation curve, due to the numerous peaks and valleys in the 5-10 kHz frequency interval that can match one or the next simulated response. However, the curves for 150 m and 225 m seem to be the closest ones to the measured curve.

The analysis of the indexes values listed in Table 14 evidences discrepancies of the indexes indications. For example: IELF and Theil indexes indicate the fourth curve as the close to measurement, while Zanazzi-Jona, Pendry and Van Hove indexes prefer the first one. Looking at the values of Theil and Pendry indexes, that give indication of the similarity of the curves in absolute way, it is evident a good but not perfect match between the curves. Values of modified Pendry index are over 0.58, due to the differences between first derivative terms of the curve to compare, while Theil coefficient has a value under 0.36 that indicate a good match between the curves absolute values.

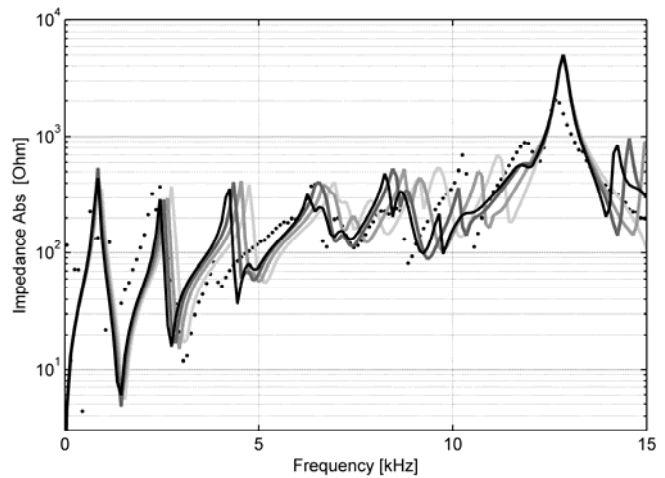


Fig. 13. Pantograph impedance for different values of feeding cables length (from light gray to black: $l_1=75 \text{ m}$, $l_2=150 \text{ m}$, $l_3=225 \text{ m}$, $l_4=300 \text{ m}$)

Table 14. Indexes for different length of supply feeding cables ($l_1=75 \text{ m}$, $l_2=150 \text{ m}$, $l_3=225 \text{ m}$, $l_4=300 \text{ m}$)

		l_1	l_2	l_3	l_4
Pendry	Theil	0.3521	0.3470	0.3407	0.3380
	R_P	0.6771	0.7001	0.7053	0.6967
	R_{PL}	0.5892	0.6077	0.6151	0.5961
Van Hove	RV	5.0077	5.4114	5.4165	5.1516
	RV_1	0.5068	0.5149	0.4768	0.4529
	RV_2	0.4881	0.5044	0.4643	0.4569
	RV_3	0.0444	0.0667	0.0242	0.0167
	RV_4	1.5808	1.6701	1.6677	1.5439
	RV_5	4.6993	5.0965	5.1102	4.8725
ZJ		0.2012	0.2364	0.2474	0.2311
IELF		98.099	94.401	88.504	84.950

In Table 15 the maximum absolute error, the mean absolute error and the root mean square between measurement and simulated curves are presented; such values indicate the third simulated impedance curve as the closest to the measurement one.

Table 15. Classical errors between curves (maximum absolute error, mean absolute error and root mean square) with respect to feeding cables length

	l_1	l_2	l_3	l_4
max	3490	3480	3470	3490
mean	167.8	159.1	147.4	152.5
rms	377.5	369.8	364.4	371.7

The simulated curves have several peaks (resonances) and valleys (anti-resonances) that, if not matching accurately the measured data, may increase the error terms and bias the overall index value. For this reason the frequency interval has

been divided in smaller sub-intervals, calculating an index separately for each of them. In this way small and larger errors are more easily recognizable and quantifiable. The sub-intervals are seven, each with at least one peak and one valley: #1 50-1350 Hz, #2 1350-3050 Hz, #3 3050-6750 Hz, #4 6750-8850 Hz, #5 8850-10550 Hz, #6 10550-12250 Hz, #7 12250-15000 Hz. The values of the indexes for each sub-interval are calculated and plotted in Fig. 14 to 19, distinguishing the variations of the parameter related to supply feeder length.

Regarding the error between the individual values of the data points, evaluated with the Theil coefficient, the worst intervals are #1, #2 and #5, where there is disagreement in the height of the resonance peaks. It is also observed that the simulated curves in #2 and #6 are more influenced by the feeding cable length.

Regarding the differences between the first derivatives, that is the slope of the curves, the Pendry and modified Pendry indexes indicate central intervals as the worst one, in agreement with Van Hove correlation factor. These intervals are those suffering most the shift of the curves and spread of values while changing the feeding cable length.

About differences in the second derivatives of the curves, measured by the Zanazzi-Jona correlation factor, the worst intervals are #1 and #2, but the reason is to be sought in noisy measurements and some weird data points (already commented, due to the influence of supply harmonics); also this index is susceptible to the variation of the feeding cables length.

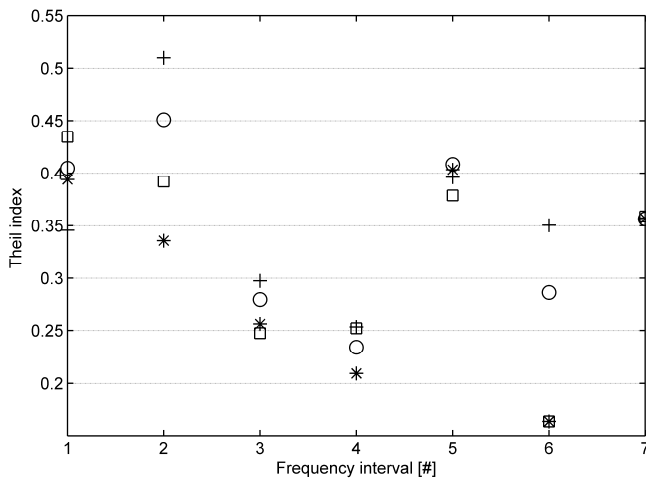


Fig. 14. Theil inconsistency coefficient for intervals #1 to #7 and different feeding cable lengths: $l_1=75$ m “cross”, $l_2=150$ m “circle”, $l_3=225$ m “square”, $l_4=300$ m “star”)

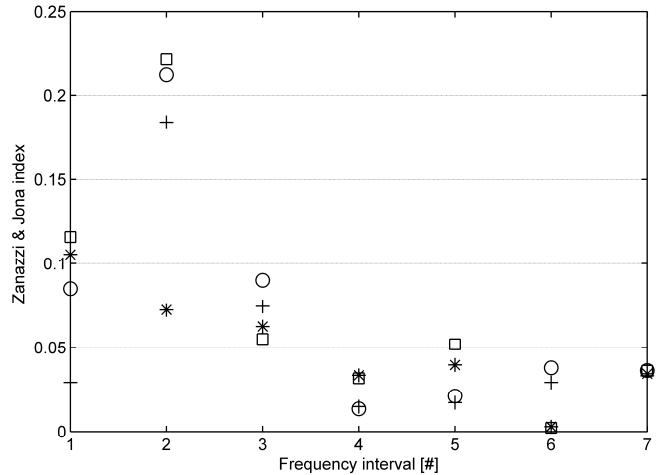


Fig. 15. Zanazzi & Jona correlation factor for intervals #1 to #7 and different feeding cable lengths: $l_1=75$ m “cross”, $l_2=150$ m “circle”, $l_3=225$ m “square”, $l_4=300$ m “star”)

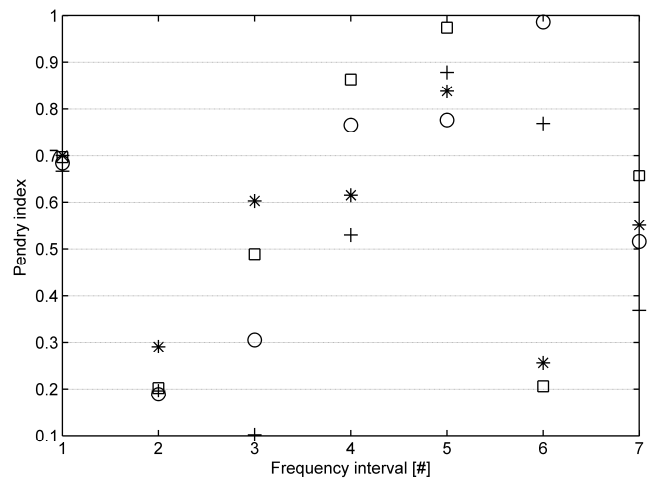


Fig. 16. Pendry correlation factor for intervals #1 to #7 and different feeding cable lengths: $l_1=75$ m “cross”, $l_2=150$ m “circle”, $l_3=225$ m “square”, $l_4=300$ m “star”)

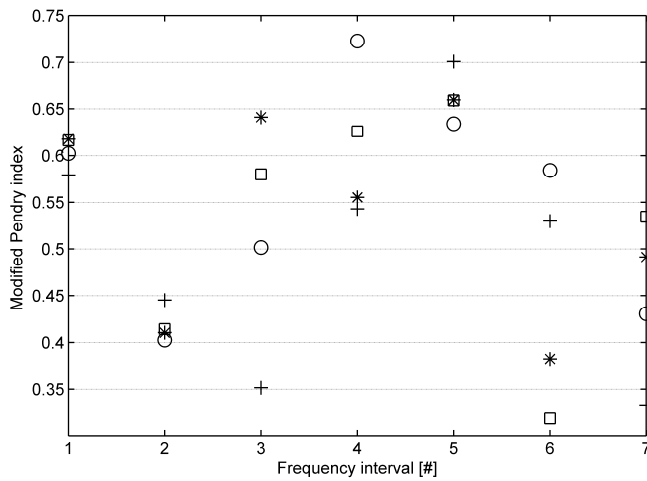


Fig. 17. Modified Pendry correlation factor for intervals #1 to #7 and different feeding cable lengths: $l_1=75$ m “cross”, $l_2=150$ m “circle”, $l_3=225$ m “square”, $l_4=300$ m “star”)

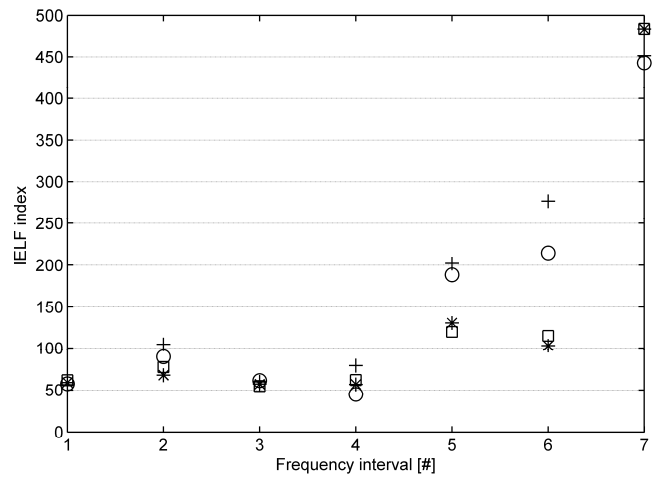


Fig. 19. IELF for intervals #1 to #7 and different feeding cable lengths: $l_1=75$ m “cross”, $l_2=150$ m “circle”, $l_3=225$ m “square”, $l_4=300$ m “star”)

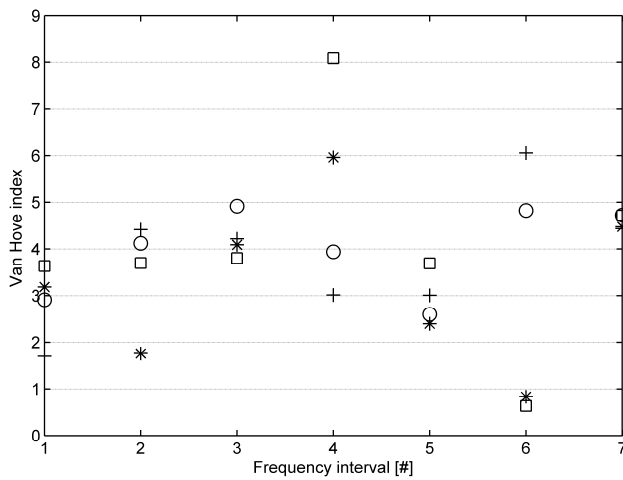


Fig. 18. Van Hove correlation factor for intervals #1 to #7 and different feeding cable lengths: $l_1=75$ m “cross”, $l_2=150$ m “circle”, $l_3=225$ m “square”, $l_4=300$ m “star”)

V. CONCLUSION

Several indexes (called in the literature “performance” or “reliability”, followed by the words “index” or “factor”), used to assess the similarity between two curves of data, have been considered and evaluated against typical examples: first synthetic examples of curves typical of time and frequency domain vectors are used and then the simulation of two electric traction lines is considered. The usefulness of these indexes is recognized for the validation of simulation models against experimental data. To this aim the desirable properties of the index are: a known range of its output value in order to assess the optimality of a curve in an absolute, rather than relative way; insensitivity to small curve defects, such as discontinuities that affect on the contrary the calculation of derivatives; wide applicability including zero-mean curves; definite behavior with respect to linearity, differences in peaks and slopes between curves, etc.

The indexes were evaluated using a sinusoidal and a triangular signal (by injecting differences such as phase difference and offset) and a dynamic system frequency response (for which the pole pair was moved by both deterministic and random quantities).

Some indexes cannot be used with zero-mean curves (Van Hove, Zanazzi-Jona) or on the contrary require the removal of any offset (Theil). Pendry index cannot be calculated if even one point only of the curves is zero. The resulting performances clearly identify some indexes (Zanazzi-Jona, Van Hove, modified Pendry and IELF) that do not suffer scale changes, keeping the same value whatever the amplification of the curves. Linearity was tested for increasing defects tracking the change of index value; we may distinguish between truly linear (Theil, modified Pendry), approximately linear (Van Hove, IELF) and non-linear (Zanazzi-Jona, Pendry) indexes.

Applying the calculation of the indexes to real case studies some considerations can be added. There is a general sensitivity to noise when derivatives are calculated; all the

authors agree in a preliminary smoothing of curves to remove noise and small artifacts.

As it is common when considering the modeling of complex systems with uncertain parameters, some deviations are accepted by experts provided that the shape and the main features are in agreement between simulations and experimental data used for validation. It is however true that when the considered curves have one or few localized deviations, such errors bias the estimation and then the indexes are useless to evaluate the similarity over the rest of the interval. To this aim curves were split in smaller intervals and for each of them indexes calculated separately, demonstrating a better interpretation of the degree of fitness of the curves and the influence of parameters on curve characteristics.

REFERENCES

- [1] M.U. Brandolini, C. Briano, E. Briano and R. Revetria, "VV&A of Complex Modeling and Simulation Systems: Methodologies and Case Studies," *International Journal of Mathematics and Computers in Simulation*, Vol. 2, n. 4, 2008, pp. 338-348.
- [2] M. Panoiu and F. Neri, "Open research issues on Modeling, Simulation and Optimization in Electrical Systems," *WSEAS Transactions on Systems*, Vol. 13, 2014, pp. 332-334.
- [3] H. Efendic, "Model-on-Demand Software Tool for Automatic Fault Diagnosis in Complex Systems," *WSEAS Transactions on Power Systems*, Vol. 6, n. 2, Feb. 2007, pp. 279-286.
- [4] S. Damangir, G. Jafarjashemi and H. Zohoor, "Modelling of a Complex System Using the Dynamic Rule Prediction," *WSEAS Transactions on Power Systems*, Vol. 5, n. 12, Dec. 2006, pp. 2833-2838.
- [5] *Railway applications – Fixed installations – Requirements for the validation of simulation tools used for the design of traction power supply systems*, CENELEC C20 working document, May 2012.
- [6] European Union, Technical Specifications for Interoperability – Energy System, 2002/733, 30-05-2002.
- [7] *Railway applications. Power supply and rolling stock. Technical criteria for the coordination between power supply (substation) and rolling stock to achieve interoperability*, CENELEC EN 50388 Standard, Aug. 2005.
- [8] A. Mariscotti, "Direct Measurement of Power Quality over Railway Networks with Results of a 16.7 Hz Network," *IEEE Transactions on Instrumentation and Measurement*, vol. 60 n. 5, May 2011, pp. 1604-1612.
- [9] A. Mariscotti, "On the validation of models of large complex electrical systems," *International Journal of Measurement Technologies and Instrumentation Engineering*, vol. 5 n. 1, Jan.-March 2015.
- [10] J. Bongiorno and A. Mariscotti, "Experimental validation of the electric network model of the Italian 2x25 kV 50 Hz railway," presented at the 20th Imeko TC4 International Symposium, Benevento (Italy), Sept. 15-17, 2014.
- [11] H. Theil, *Economics and Information Theory*, Amsterdam, North-Holland, 1967.
- [12] E. Zanazzi and F. Jona, "Reliability factor for surface structure determination," *Surface Science*, Vol. 62 no. 1, pp. 61-80, 1977.
- [13] J.B. Pendry, "Reliability factors for LEED calculations," *Journal of Physics – Part C: Solid State Physics*, Vol. 13, pp. 937-944, 1980.
- [14] J. Bongiorno and A. Mariscotti, "Performance of indexes used for model validation," Proceedings of CSECS 2014, Lisbon, Portugal, Oct. 30 – Nov. 01, 2014.
- [15] M.A. Van Hove, S.Y. Tong and M.H. Elconin, "Surface structure refinement of 2H-MoS₂ via new reliability factors for surface crystallography," *Surface Science*, Vol. 64 No. 1, pp. 85-95, 1977.
- [16] R.J. Simpson, C.R. Jones, I. MacDiarmid, A. Duffy and D. Coleby, "The integrated error against log frequency (IELF) method for CEM validation," presented at the IEEE International Symposium on Electromagnetic Compatibility, Aug. 8-12, 2005, Chicago, USA, pp. 296-300.
- [17] D. Coleby and A. Duffy, "Analysis of techniques to compare complex data sets," *COMPEL - The international Journal for Computation and Mathematics in Electrical and Electronic Engineering*, Vol. 21 No. 4, pp. 540-553.
- [18] A. Mariscotti and P. Pozzobon, "Experimental results on low rail-to-rail conductance values," *IEEE Transactions on Vehicular Technology*, vol. 54 n. 3, May 2005, pp. 1219-1222.
- [19] A. Mariscotti and P. Pozzobon, "Measurement of the Internal Impedance of Traction Rails at Audiofrequency," *IEEE Transactions on Instrumentation and Measurement*, vol. 53 n. 3, June 2004, pp. 792-797.
- [20] A. Mariscotti and P. Pozzobon, "Synthesis of line impedance expressions for railway traction systems," *IEEE Transactions on Vehicular Technology*, vol. 52 n. 2, March 2003, pp. 420-430.